Improved anisotropy measurement of the Lamb shift in He^+

J. Patel, A. van Wijngaarden, and G. W. F. Drake
Department of Physics, University of Windsor, Windsor, Ontario, Canada N9B 3P4
(Received 9 July 1987)

An improved anisotropy measurement of the Lamb shift is obtained by means of a new method for the high-precision measurement of light intensities. The photon-counting techniques used in our previous work [Phys. Rev. A **20**, 1299 (1979)] are replaced by the direct measurement of photoelectron currents with high-precision electrometers. Our new value for the Lamb shift in He^+ is 14 041.9±1.5 MHz. This agrees with the earlier microwave resonance measurement of Lipworth and Novick [Phys. Rev. **108**, 1434 (1957)], but lies clearly below the more recent measurement by Narasimham and Strombotne [Phys. Rev. A **4**, 14 (1971)].

I. INTRODUCTION

The Lamb shift in one-electron atoms remains one of the most important tests of quantum electrodynamics (QED) and the underlying assumptions concerning the nature of electromagnetic interactions.[1] The most accurate measurements to date are for the $2s\ ^2S_{1/2}-2p\ ^2P_{1/2}$ splitting of neutral hydrogen, obtained by variations of the microwave resonance technique originally pioneered by Lamb and Retherford.[2] However, the value recently reported by Lundeen and Pipkin[3] (±9 ppm) is not in good agreement with theory.[4–6]

We are continuing to develop an alternative method of measuring the Lamb shift, which is based on the observation that when a hydrogenic atom in the metastable $2s\ ^2S_{1/2}$ state is quenched by a static electric field, the induced Ly-α intensities $I_\parallel$ and $I_\perp$ emitted in the directions parallel and perpendicular to the electric field are not equal. The anisotropy defined by

$$R=(I_\parallel-I_\perp)/(I_\parallel+I_\perp) \tag{1}$$

is (nearly) proportional to the Lamb shift. For all low-Z hydrogenic ions, $R\simeq 0.1$, and the value of R is independent of field strength in the limit of weak fields. As described in detail previously,[7,8] the intensity ratio $r=I_\parallel/I_\perp$ is measured at a single point along a beam of metastables. By rotating the electric field in steps of 90°, the data can be combined in such a way that the relative sensitivities of the detectors, and many other systematic effects, cancel out. An advantage of the anisotropy method is that it is insensitive to the width and shape of the resonance, and it therefore provides an independent check of microwave resonance measurements.

The purpose of the present paper is to report a new method for the high-precision measurement of the light intensities in (1), and a new value for the Lamb-shift anisotropy in He^+ which is more accurate (±105 ppm) than our previous work[8] by a factor of 2. We previously measured $I_\parallel$ and $I_\perp$ by photon-counting techniques. We have since found that a ±200-ppm uncertainty is about the limit of what can be achieved with conventional photomultipliers or channeltron detectors.

The problem is that the sensitivity of electron multipliers is slightly dependent on the count rate due to changes in the pulse-height distribution, and hence the output is weakly nonlinear. This introduces a systematic error which cannot be removed because there are no known calibrating sources of sufficient linearity. Furthermore, the nonlinearity itself is unstable, as it depends on the gain of the electron multiplier.

We have now circumvented this problem by eliminating photon counting and instead measuring directly the photoelectron current emitted by a detector surface without any intermediate amplification stage. Since no photoelectron cascade stage is involved, nonlinearities due to surface changes are not introduced.

There are several reasons for using He^+ instead of H for the anisotropy measurement. First, since the percentage theoretical uncertainty in the electron self-energy contribution to the Lamb shift scales as Z^2, a measurement in He^+ need be only one-fourth as accurate as a measurement in H to provide an equivalent test of theory. Second, there is no hyperfine structure for $_2He^4$ to complicate the analysis of the quenching signal. Third, the nuclear radius of $_2He^4$ is known to exceptionally high precision from fine-structure measurements in the muonic system μ^--He^{2+},[9] while a similar precision is not available for the proton or other nuclei. Consequently, the uncertainty due to the finite-nuclear-size correction is greatly reduced.

An additional reason for studying He^+ is that the two existing microwave resonance measurements of 14 040.2±1.8 MHz (Ref. 10) and 14 046.2±1.2 MHz (Ref. 11) for the Lamb shift are in disagreement with each other. The accuracy of our anisotropy Lamb shift is now ±1.5 MHz, which is sufficient to distinguish between the above two values. As further discussed below, there are excellent prospects that the uncertainty can be further reduced to the ±10-ppm level (±0.15 MHz), which would provide a definitive test of theory.

II. APPARATUS AND PROCEDURE

A. Overall plan

Although the anisotropy method has been described in detail in Refs. 7 and 8, significant modifications in the

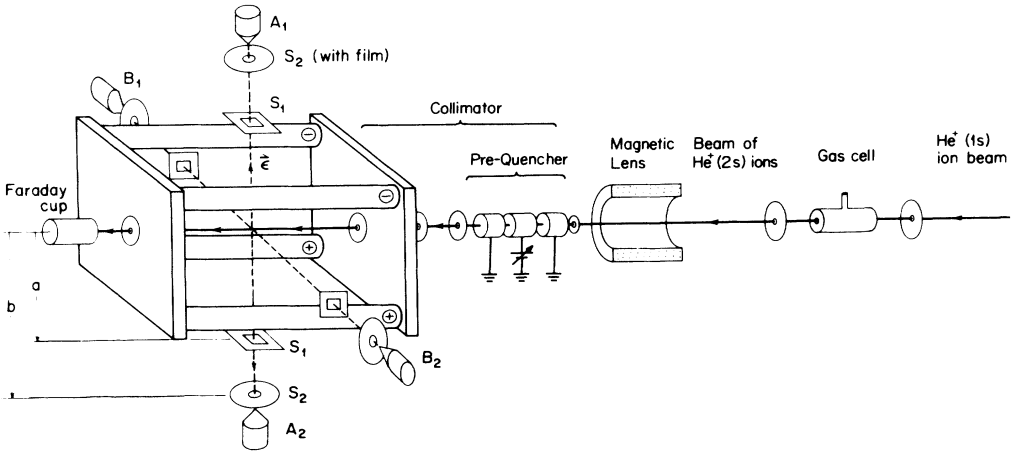

FIG. 1. Schematic diagram of the apparatus (not to scale) used to measure the anistropy. The four metal rods in the quenching cell each have a diameter of (1.2700±0.0002) cm and are supported (4.064±0.001) cm apart on insulators. The length of the quenching cell is 15.24 cm. Slits S_1 and S_2 for the photon collimator (shown in Fig. 2) are mounted at distances $a = 7.112$ cm and $b = 21.84$ cm from the beam axis.

equipment illustrated in Figs. 1 and 2 need description. A He^+-ion beam containing about 0.5% metastable ions is formed by passing a beam of 121.5-keV ground-state He^+ ions, from a magnetic mass analyzer, through a gas cell. The emerging beam enters a magnetic lens consisting of an axial magnetic field region produced by a 25-cm-long coil. This lens improves the final beam current through the collimator into the quenching cell by an order of magnitude, at an optimum magnetic field of 6000 G in the center of the coil. On leaving the lens, the beam passes through the circular opening of the electrodes of a prequencher, a collimator that limits the beam diameter to 0.16 cm, and finally enters the quadrupole field region in the observation cell, where a static electric field is produced by supplying opposite polarities to two pairs of cylindrical conducting rods mounted on insulators. The quenching cell is at a distance of 210 cm, corresponding to a flight time of 900 ns, from the exit of the gas cell. In the quadrupole field the induced Ly-α radiation emitted perpendicular and parallel to the field direction is detected simultaneously by measuring the photoelectric current from the photosensitive cones, labeled A_1, A_2, B_1, and B_2. Detection periods are normalized by monitoring the beam current with a Faraday cup. All data were taken at a single quenching field strength of 632.8 V/cm, obtained by applying 1450.5 V of opposite polarity to opposite pairs of the quadrupole rods.

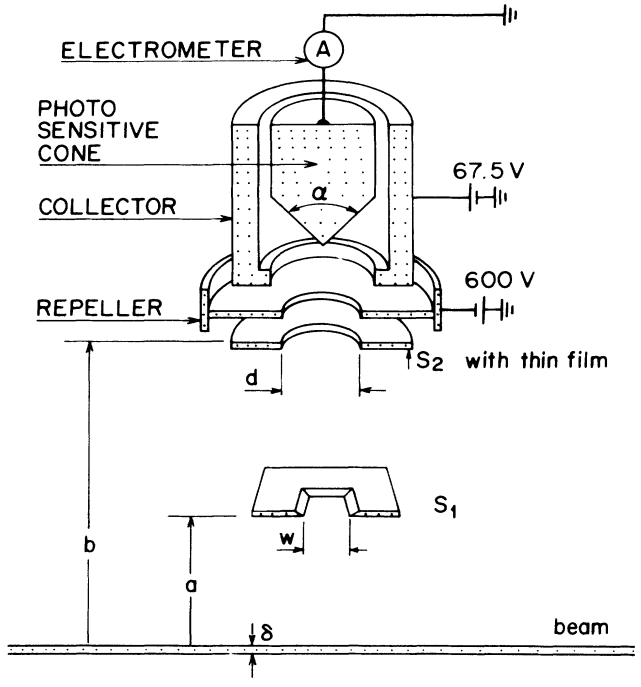

FIG. 2. Details of the photon-detection system from Fig. 1, where the distances a and b are defined.

B. Gas cell

In previous work[8] with no magnetic lens, He was leaked into the gas cell rather than a high-Z gas to obtain a maximum current component of metastable ions in the beam, after collimation. With the lens in place, however, a higher metastable current was obtained by leaking N_2 (or air) into the gas cell. The increased yield for N_2 arises from the focusing action of the lens. It compensates for the greater current loss that results from the larger angular divergence of a fast ion beam after traversing a higher-Z gas.

Although the gas cell, operating at a pressure near 10^{-3} Torr, is differentially pumped to keep the pressure in the observation region as low as possible, the cell nevertheless presented a sizeable gas load. Leaking gas into it makes the pressure rise from 4×10^{-8} Torr to 7.5×10^{-8} Torr.

The vacuum system itself is strongly baffled with liquid-nitrogen-cooled traps above the diffusion pumps, operating with Santovac 5 fluid. One large liquid-nitrogen trap is mounted directly underneath the gas cell. Other traps are located near the entrance and exit slits of the collimator, and finally a large trap is mounted inside the observation chamber, near the quenching cell. A consequence of strong trapping is that the residual gas in the quenching cell consists primarily of N_2 gas (introduced by the gas load) and some water vapor. Since we do not bake our vacuum system, the water-vapor wall load remained virtually constant throughout the duration of the experiment.

C. Reduction of beam contamination

Leaving the gas cell are He^+ ions in several excited states that, with the exception of the long-lived metastable $2s$ state, have a short lifetime and decay, forming ground-state He^+ ions. There are also neutral He atoms produced in charge-changing collisions. This mixture of states is then steered into the collimator which is rigidly attached to the quenching cell. Small mechanical adjustments in the position of the gas cell and the lens allow alignment of the beam. The presence of small magnetic stray fields from the mass-analyzing magnet near the gas cell and lens separate the charge components from the neutrals. No attempt was made to cancel the fields here, but they instead were used to advantage for removing neutrals from the beam entering the quenching cell. This not only reduces the background noise signal but also assures that the observed anisotropy is not affected by field-dependent decays of excited He atoms.

The concentration of long-lived He^+ excited states with $n>2$, for which the lifetime is field dependent, must also be kept small. This was accomplished as follows. Since the cross section for excitation of He^+ ground-state ions in passing through the gas cell varies approximately as n^{-3} for $n>3$,[12,13] the production of excited states with, say, $n>6$ will be small. For $n=6$, the lifetime for cascading to the ground state is 38 ns (Ref. 14) which is small compared with the long flight time of 900 ns from the gas cell to the observation region. Moreover, the beam first passes through a field of 100 V/cm maintained between the electrodes of the prequencher for a period of 63 ns and then travels half the length of the quenching cell in the quadrupole quenching field before reaching the observation region. These fields reduce the concentrations of long-lived highly excited states that might survive the flight time of 900 ns from the gas cell to the observation point.

D. Photon detection

Details of the photon-detection system are shown in Fig. 2. The quench radiation from the beam successively passes through a rectangular slit S_1 of width $w=1.240$ cm, a circular slit S_2 of diameter $d=1.016$ cm, the circular opening of a repeller plate kept at -600 V, and then strikes the photosensitive cone with cone angle α. The photoelectrons are collected onto a cylindrical surface kept at $+67.5$ V and the photocurrent is measured with an electrometer (Keithley Model 642 LNFA) which by itself has a rms dark current of 4×10^{-17} A.

The polished metallic surface of the photon-sensitive cone is coated with a thin layer of MgF_2 to enhance[15] the photoelectric yield. The yield is independent of the thickness of the coating for thickness $t<100$ Å investigated, provided that there is at least a monolayer. Under these conditions the yield was found to be the same for coated cones of Mg or Al. The MgF_2 layer raises the efficiency by a factor 2 and, for angles of incidence less than 45°, the absolute photon-detection efficiency should be[15] about 20%.

With a He^+ beam current of 5 μA ($\sim0.5\%$ metastable ions) and a quenching field $F=632.8$ V/cm, the observed photocurrent per detector is 3×10^{-14} A, which is large compared with the noise current of 4×10^{-17} A of the electrometer. In our present work, opposite pairs of cones were connected by a 150-cm-long cable and their combined photocurrent output fed into a single electrometer. A low-noise coaxial cable was constructed out of an outer copper pipe in which the inner conductor was coaxially supported on sapphire insulators. An electronic rms noise of $(2-3)\times10^{-16}$ A still generated by these cables yields a signal-to- (electronic) noise ratio no better than one part in 250.

A potential source of electronic noise are the power supplies for the electrodes near the cones. Since variations in voltages of 0.05 mV or less resulted in prohibitively large induced current variations, the power supplies were replaced by dry cells. The precise values of their emf's are unimportant. For example, the measured photocurrent was found to be the same for collector potentials of 22.5, 45, and 67.5 V.

The output of the two electrometers for detection systems A and B (see Fig. 1) were each connected to a digital voltmeter (Hewlett Packard Model 3457A). Their outputs were sampled at a low rate of three times per second, governed by the slow response of the electrometers to current changes. The readings were normalized to the ion beam current and stored in a computer. This procedure allowed the precise determination of the noise current for the same beam flux as for the corresponding signal.

E. Elimination of particle noise

A difficulty in the experiment arises from the many charged particles and metastable species produced by the fast He^+ ion beam in passing through the residual gas in the quenching cell. The charged particles are accelerated by the quenching field and if they are allowed to strike the photosensitive cones, the magnitude of the resulting noise would be dependent on the direction of the quenching field, producing a false anisotropy. The detection system has therefore been designed to filter out charged particles so that only photons, in particular the 304-Å Ly-α radiation, are detected.

Metastable particles and low-energy ions are prevented from striking the cones by a self-supporting thin Al film mounted over the circular openings of slits S_2. The film is sufficiently thin that absorption of the 304-Å

photon is small. Low-energy electrons are kept away by the negatively biased (−600 V) repeller plate (Fig. 2). Higher-energy electrons would produce soft x rays on striking the film. This is avoided by means of a pair of Helmholtz coils that provide an axial magnetic field of 12 G along the beam direction.

Two other pairs of Helmholtz coils cancel the earth's and other stray magnetic fields near the observation region. Their purpose is to ensure the absence of motional $\mathbf{v}\times\mathbf{B}/c$ electric fields.

F. Reduction of polarization effects

The anisotropy method requires a measurement of the total intensities $I_{\parallel}$ and $I_{\perp}$ summed over photon polarizations. The $I_{\parallel}$ component is unpolarized, but $I_{\perp}$ has a polarization given by $P=2R/(1-R)$.[16] For He^+, $P=0.26$. One must therefore ensure that the detectors respond equally to different polarizations.

The cylindrical symmetry of the detector cones guarantees polarization insensitivity for a point light source on the cone axis. However, for our extended line source defined by slits S_1 and S_2 in Fig. 2, the range of possible angles between the cone surface and the electric field vector of radiation from off-axis points is polarization dependent. The resulting polarization sensitivity is small for large cone angles and small viewing sections of the ion beam.

Since smaller cone angles yield a larger detection efficiency,[15] there is a trade-off between maximizing efficiency and minimizing polarization sensitivity. In preliminary studies we found that the efficiency for a cone angle $\alpha=54°$ is 50% larger than that for a cone angle of 90°. However, with the 54° cone and a slit S_1 of width $w=1.24$ cm, effects resulting from the residual polarization sensitivity were detectable. These could no longer be observed when w was decreased to 0.64 cm. From an analysis of these results, it was concluded that for cone angles $\alpha\gtrsim 90°$ and a slit S_1 of width $w\lesssim 1.24$ cm, the polarization sensitivity is negligibly small. Further experimental verification of this conclusion is given in Sec. IV.

For our detection systems, the absolute photon efficiencies are not the same but differ by as much as 0.1%. The difference can be accounted for by the variations in photoabsorption in the thin Al films (on the S_2 slits) whose thicknesses were only approximately kept the same.

G. Measurement of $I_{\parallel}/I_{\perp}$

We now describe the procedure for measuring the intensity ratio. Since opposite cones (Fig. 1) are connected to one electrometer, we denote by A the combined photocurrents from detectors A_1 and A_2, and by B the corresponding total output current from the other two cones. We also assume that A and B are measured simultaneously and represent time-average photocurrents.

By switching the polarities on the quadrupole rods, the direction of the quenching field can be rotated by 90°. Let θ $(=0,\pi/2,\pi,3\pi/2)$ be the angle between the electric field and the A_2A_1 axes in Fig. 1 with the convention that angles are positive for counterclockwise rotations when viewed along the incoming ion beam direction. The only possible intensity ratios $r(\theta)$ of the form $I_{\parallel}/I_{\perp}$ that can now be measured are

$$\frac{A(0)}{B(0)},\quad \frac{B(\pi/2)}{A(\pi/2)},\quad \frac{A(\pi)}{B(\pi)},\quad \frac{B(3\pi/2)}{A(3\pi/2)}\ .$$

These ratio values would be the same if the four detectors were equally efficient. Since they are not, we form an angle-averaged r value,

$$r=\left[\frac{A(0)}{B(0)}\frac{B(\pi/2)}{A(\pi/2)}\frac{A(\pi)}{B(\pi)}\frac{B(3\pi/2)}{A(3\pi/2)}\right]^{1/4}, \tag{2}$$

which is completely independent of the efficiencies of the detectors.

H. Noise corrections

The measured photocurrents $A(\theta)$ and $B(\theta)$ from quenching need to be corrected for noise. At our (average) operating pressure of 7.5×10^{-8} Torr, this noise consists of about equal parts of a pressure-dependent background photon noise and a constant electronic noise, discussed in Sec. II D. The photon noise originates from a "glowing column" of excited atoms and excited ions created in the residual gas along the trajectory of the fast primary He^+ beam, and is proportional to the gas pressure. This photon noise is also slightly anisotropic since upon application of a quenching field, the secondary positive ions are pushed into the direction of the field, towards one of the detectors and away from the opposite detector. This results in a field-direction-dependent photon noise which is isotropic only in first order.

There are now two ways to correct for the anisotropic part of the noise. The first method, adopted in this work, begins by defining the isotropic noise as the signal current still observed in the absence of the quenching field, with all the quadrupole rods grounded. When the noise measurements $a(\theta)$ and $b(\theta)$ so obtained are subtracted from the corresponding signals $A(\theta)$ and $B(\theta)$ in Eq. (2) with the field switched on, then the resulting r value depends on pressure. The reason is that the pressure-dependent anisotropic part of the noise present in the signal has not been subtracted from the numerator in Eq. (2). Since the anisotropic part of the noise itself is proportional to pressure, we find that for a large signal-to-noise ratio, the pressure dependence of the intensity ratio is given by

$$r(p)=r(0)+(dr/dp)p\ . \tag{3}$$

Here $r(0)$ is the pressure-corrected value for the $I_{\parallel}/I_{\perp}$ ratio.

Thus $r(0)$ can be found by accurately measuring $r(p)$ at the lowest achievable pressure, together with a few less accurate values at much higher pressure. An extrapolation of the r-p plot to zero pressure then yields $r(0)$.

In practice $r(p)$ was measured at the lowest achievable pressure a large number (6225) of times, where a single measurement consists of signal determinations for the

four possible field orientations. Since the electronic part of the noise exhibited slow drifts, a single noise determination was made along with each measurement.

The second way to correct for noise defines it as the signal still observed in the presence of quenching field for an ion beam without metastable ions. In practice such a beam is obtained by raising the polarities on the prequencher (see Fig. 1) to a sufficiently high level to destroy virtually all the $2s$ states. This noise definition automatically accounts for the anisotropic part of the noise, but it requires that a noise measurement be made at each of the four field orientations for a single r value, instead of a single noise measurement, as in the first method. Though this second method, used in previous work,[8] avoids a pressure-dependent r value and its associated difficulties, it is more time consuming and has, therefore, not been used in our present measurement of the Lamb shift.

III. THEORY

In this section only the theoretical results[8,9] relating the Lamb shift

$$\mathcal{L}=E(2p_{1/2})-E(2s_{1/2}) \tag{4}$$

to the anisotropy $R=(r-1)(r+1)$ are summarized. The anisotropy is nearly proportional to the ratio of the Lamb shift to the fine-structure splitting. It can be expressed in terms of

$$\rho=\frac{E(2s_{1/2})-E(2p_{1/2})+\frac{1}{2}i\Gamma_p}{E(2s_{1/2})-E(2p_{3/2})+\frac{1}{2}i\Gamma_p}\ , \tag{5}$$

where Γ_p is the level width of the $2p$ state. In the limit of weak field, the anisotropy is

$$R^{(0)}=\frac{[-3\,\mathrm{Re}(\rho)-\frac{3}{2}|\rho|^2]}{[2-\mathrm{Re}(\rho)+\frac{7}{2}|\rho|^2]}\ , \tag{6}$$

and for finite fields ε it becomes

$$R=R^{(0)}+R^{(2)}\varepsilon^2+R^{(4)}\varepsilon^4\ . \tag{7}$$

Small corrections arise from (a) contribution to the quench radiation via intermediate p states with $n>2$ and from final-state perturbations, (b) relativistic and retardation corrections of order α^2Z^2 to the electric dipole radiation, and (c) a magnetic quadrupole ($M2$) decay mode $2s_{1/2}-2p_{3/2}-1s_{1/2}$. With these, the final asymmetry becomes

TABLE I. Input data for calculating the $2He^+$ anisotropy.

$E(2p_{3/2})-E(2p_{1/2})$	175 594.0 MHz
$\Gamma(2p)$	$1.0028\times10^{+10}$ sec^{-1}
$R^{(2)}$	5.822×10^{-4} (kV/cm)$^{-2}$
$R^{(4)}$	-3.7×10^{-6} (kV/cm)$^{-4}$
ε	0.6328 kV/cm
$\left[\frac{\delta R}{R^{(0)}}\right]_p$	-2.37×10^{-5}
$\left[\frac{\delta R}{R^{(0)}}\right]_{\mathrm{rel}}$	0.64×10^{-5}
$\left[\frac{\delta R}{R^{(0)}}\right]_{M2}$	-6.54×10^{-5}

$$R=R^{(0)}\left[1+\left[\frac{\delta R}{R}\right]_p+\left[\frac{\delta R}{R}\right]_{\mathrm{rel}}+\left[\frac{\delta R}{R}\right]_{M2}\right]$$
$$+R^{(2)}\varepsilon^2+R^{(4)}\varepsilon^4\ . \tag{8}$$

Using the input data in Table I, the theoretical anisotropy for the Lamb shift $\mathcal{L}=14\,042.36$ MHz predicted by Mohr[4] becomes

$$R^{(0)}=0.117\,968\,0\ . \tag{9}$$

IV. RESULTS AND ANALYSIS

A. Observed ratio

The results for three sets of ratio measurements obtained at the lowest achievable residual pressure of $(7.5\pm0.5)\times10^{-8}$ Torr are given in the fourth column of Table II. The total of 6225 individual measurements were obtained in 52 separate runs, on different days, each containing an average of 120 measurements. For most of them (3906), the cone angle was $\alpha=90°$ and the width of the entrance slit S_1 to the photon collimator shown in Fig. 2 was $w=(1.240\pm0.003)$ cm.

As discussed in Sec. II E, the measured r value should depend neither on the length of the viewing section of the He^+ beam nor on the cone angle. To verify this, an additional 1613 measurements were made with a smaller slit width ($w=0.991\pm0.003$ cm) and another 706 mea-

TABLE II. Observed intensity ratio at a pressure of $p_0=(7.5\pm0.5)\times10^{-8}$ Torr.

Cone angle α (deg)	Slit width w (cm)	Number of measurements	Ratio r	Ratio r corrected for solid angle
90	0.991	1613	1.267 874	1.268 139±0.000 051
90	1.240	3906	1.267 705	1.268 092±0.000 036
120	1.240	706	1.267 720	1.268 042±0.000 094
			Average ratio	1.268 098 3±0.000 028 0

surements with a larger cone angle $\alpha = 120°$.

Results for the first two sets of measurements in the table cannot be directly compared because their slit functions differ. The solid angle correction for the anisotropy previously described[8] for the case that both slits S_1 and S_2 are rectangular only slightly differs from that of the present experiment where S_2 is circular. The corrected anisotropy is now related to the observed anisotropy R_0 as

$$R = R_0 \left[1 + (1-R) \frac{w^2 + 3d^2/4}{12(b-a)^2} + \frac{3d^2/4}{6b^2} + \frac{\delta^2}{8b^2} \right], \quad (10)$$

where the meaning of the various symbols is shown in Fig. 2. This relation, together with Eq. (1), has been used to find the solid angle corrected ratios in the last column of Table II. Since these values agree with each other within error, they have been combined to yield an average

$$r(p_0) = 1.268\,098\,3 \pm 0.000\,028\,0 \, . \quad (11)$$

B. Statistical error

Instabilities in the electronic noise level posed a difficulty in the determination of the statistical error. The overall noise exhibited a symmetric but non-Gaussian behavior with larger fluctuations occurring more frequently than what would be expected for a normal distribution. This feature translates itself into the histogram (Fig. 3) for the 6225 individual measurements. The dotted curve consists of the sum of three weighted Gaussian distributions for the three results from Table II. As expected, it provides but a poor fit. The χ-square test with the mean as the only adjustable parameter yields $\chi^2 = 45$ for 36 degrees of freedom corresponding to a confidence level of only 14%. A consequence of the non-Gaussian histogram is that our weighted Gaussian fit overestimates the statistical error due to abnormally large contributions from the wings. Since over a long run of measurements the (larger) noise fluctuations average to zero, a more reliable error estimate was obtained from the distribution of the 52 run averages taken as independent measurements. The corresponding errors thus found are the ones quoted in Table II and lie about 10% below those for the fit to the histogram.

Slow drifts in electronic noise do not shift the average r value, provided that the frequency distribution for low and high measurements remains the same throughout the entire duration of the experiment. Evidence that this is indeed the case is provided by the runs test (Table III) where the data reveal no statistically significant anomalies.

The final statistical run mean error in Table II arises primarily from rms electronic noise, while contributions from fluctuations in the (large) signal current are small. Thus on reducing the ion beam current, the standard deviation for the distribution of individual measurements is found to be almost inversely proportional to the signal photo current. Modifications to our apparatus that triple the photocurrent for the next generation of experiments would allow us to reduce the statistical error by an order of magnitude in a time equal to that for the present experiment.

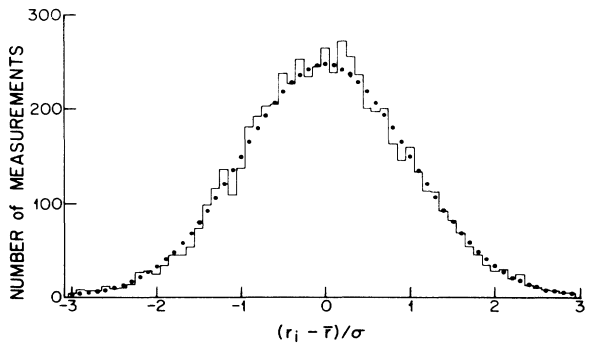

FIG. 3. Histogram for the distribution of the experimental data about the mean in units of the average expected standard deviation. The solid circles show the expected bar heights for the sum of three Gaussian distributions corresponding to the three sets of results from Table II.

C. Pressure correction

The pressure dependence for the observed ratio is shown in Fig. 4. The point at the lowest pressure $p_0 = (7.5 \pm 0.5) \times 10^{-8}$ Torr is the average value for the results in Table II. Its error bar is too small to show. The other points, with the exception of one at highest pressure, were obtained by deliberately leaking N_2 in the observation cell, since the residual gas at the lowest pressure consists primarily of that gas (and some water vapor), as discussed in Sec. II B. All pressures were monitored with the same ionization gauge. The N_2 pressure data, shown as circles, are well represented by a straight-line fit through the lowest pressure point. The point at highest pressure was obtained by leaking water vapor into the observation cell. Since the sensitivity of an ion gauge is the same[17] for N_2 and H_2O, this result is

TABLE III. Results of the runs test for the number of low and high runs.

Run length	Low runs	High runs	Expected number
1	785	768	778±24
2	362	391	389±18
3	192	192	195±13
4	98	81	97±9
5	49	59	49±6
6	25	29	24±5
7	13	14	12±3
8	9	5	6.1±2.4
9	5	2	3.0±1.7
10	1	0	1.5±1.2
11	1	1	0.76±0.87
12	1	1	0.38±0.61
13	0	0	0.19±0.44
14	1	0	0.10±0.31
Total	1542	1543	1556±20

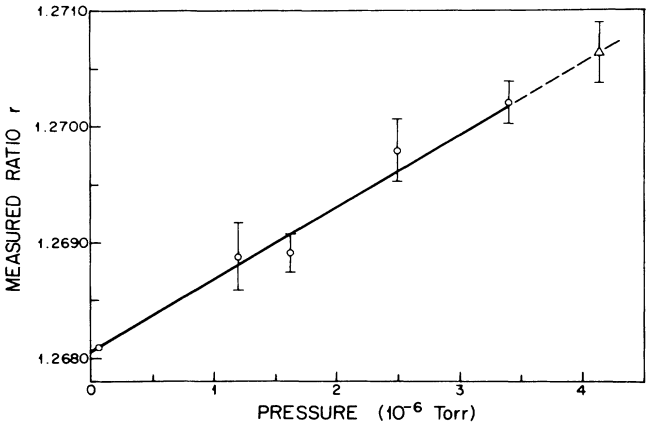

FIG. 4. The dependence of r on residual gas pressure for N_2 (circles). The straight-line fit is extrapolated through the single point (triangle) for H_2O vapor.

shown on the same graph. Although there is no *a priori* reason to expect the water-vapor point to lie on the straight-line fit for N_2, it is satisfying that it does because now the relative concentrations for these gases in the observation region need not be known.

Extrapolation of the N_2 fit to zero pressure is accomplished by multiplying the $p_0=7.5\times10^{-8}$-Torr result by the pressure correction factor

$$f_p=\left[1-\frac{p_0}{r(p_0)}\frac{dr}{dp}\right] . \tag{12a}$$

Its numerical value is

$$f_p=[1-(36.7\pm2.5)\times10^{-6}] . \tag{12b}$$

D. Relativity correction

The observed intensity ratio of the form $r=I_{\parallel}/I_{\perp}$ depends on the velocity of the He^+ ions. This is because the radiation that is observed in the laboratory frame along the electric field direction is emitted by the particle under a small angle $\theta\simeq v/c$. By contrast, $I(\pi/2)$ is not affected because of the rotational symmetry of the quench radiation perpendicular to the field direction. The correction factor multiplying the observed ratio is

$$f_{\rm rel}=[1+(v/c)^2(r-1)/r] . \tag{13a}$$

Its numerical value in this work is

$$f_{\rm rel}=[1+(13.79\pm0.05)\times10^{-6}] . \tag{13b}$$

E. Beam-bending correction

As the He^+ ions traverse the quenching cell, they undergo a displacement in the direction of the quenching field. For the parameters in this experiment, the deflection in the center of the observation region is $\Delta=0.056$ cm. This deflection alters the observed ratio in second order through a change in the observation direction perpendicular to the field, a variation in luminosity at the cones resulting from alterations in distance to the beam, and a variation of the length of the viewing section of the beam for those detectors that monitor $I_{\parallel}$. The correction factor multiplying the observed ratio is

$$f_b=[1-(3-r)(\Delta/b)^2] . \tag{14a}$$

Its numerical value in this work is

$$f_b=[1-(11.5\pm0.5)\times10^{-6}] . \tag{14b}$$

Other corrections resulting from a depletion by quenching of the metastable content along the viewing section of the beam, and changes introduced by the magnetic field splitting of energy levels in the 12-G field in the observation region were calculated and found to be negligibly small.

TABLE IV. Sources of error in the measurement of R.

Parameter	$\delta R/R$ (ppm)
Statistics	105
Solid angle correction	4
Pressure correction	9
Beam-bending correction	2
Relativity correction	0.2
Total	105.5

F. Analysis

The value of the ratio $r(p_0)$ obtained at the residual pressure p_0, when corrected for finite pressure, relativity effects and beam bending is $r=1.268\,054\,6\pm0.000\,028\,2$. This corresponds to an asymmetry

$$R=0.118\,187\,02\pm0.000\,012\,5 . \tag{15}$$

The sources of error to R are summarized in Table IV, where it is apparent that the dominant source of error arises from the statistical uncertainty.

The field-independent part of the experimental asymmetry is,

$$R^{(0)}=0.117\,964\,2\pm0.000\,012\,4 , \tag{16}$$

in agreement with theory [Eq. (9)].

TABLE V. Comparison of experimental and theoretical Lamb shifts for He^+ (MHz).

Experiment	Theory
14 041.9±1.5[a]	14 042.36±0.55[b]
14 040.9±2.9[c]	14 045.12±0.55[d]
14 040.2±1.8[e]	
14 046.2±1.2[f]	

[a] Present work.
[b] Mohr (Ref. 4).
[c] Previous work (Ref. 8), corrected for relativity effects.
[d] Erickson (Ref. 5).
[e] Lipworth and Novick (Ref. 10).
[f] Narasimham and Strombotne (Ref. 11).

V. DISCUSSION

The experimental value $R^{(0)}$ corresponds to a Lamb shift of 14 041.9±1.5 MHz. This is compared with other experimental and theoretical values in Table V.

In our previous work[8] in He^+ we neglected to take the relativity correction into account. Doing this raises the value from 14 040.2±2.9 to 14 040.9±2.9 MHz, as shown in Table V. With the exception of the measurements of Narasimham and Strombotne,[11] our Lamb-shift measurement is in agreement with the other measurements and with the calculations of Mohr.[4] It lies below the Erickson theory;[5] a trend that is also shown by the most accurate existing measurements in the heavier hydrogenic systems of $^{31}P^{14+}$ (Ref. 18), $^{35}Cl^{16+}$ (Ref. 19), and $^{40}Ar^{17+}$ (Ref. 20). All of these yield Lamb shifts which lie slightly below the predictions of Mohr. However, the most accurate existing measurement for H (Ref. 3) lies lower by four error bars. Thus high-precision measurements should be extended to heavier ions.

It is believed that the accuracy of the present experiment can be improved by an order of magnitude to meet this requirement. To this purpose, we plan to mount an additional set of four detectors in the quenching cell. These, together with other modifications, will improve the present signal-to-noise ratio by at least a factor of 3. This by itself could reduce (see Sec. IV B) the statistical error by an order of magnitude. In addition, the large cable noise can be eliminated by mounting a second pair of electrometers. These improvements could make the anisotropy method superior to existing resonance-type experiments for He^+.

[1]For a review, see G. W. F. Drake, Adv. At. Mol. Phys. **18**, 399 (1982), and earlier references therein.

[2]W. E. Lamb, Jr. and R. C. Retherford, Phys. Rev. **72**, 241 (1947).

[3]S. R. Lundeen and F. M. Pipkin, Phys. Rev. Lett. **46**, 232 (1981).

[4]P. J. Mohr, in *Beam Foil Spectroscopy,* edited by I. A. Sellin and D. J. Pegg (Plenum, New York, 1976), p. 89.

[5]G. W. Erickson, Phys. Rev. Lett. **27**, 780 (1971); J. Chem. Phys. Ref. Data **6**, 831 (1977).

[6]J. Sapirstein, Phys. Rev. Lett. **47**, 1723 (1981).

[7]A. van Wijngaarden and G. W. F. Drake, Phys. Rev. A **17**, 1366 (1978).

[8]G. W. F. Drake, S. P. Goldman, and A. van Wijngaarden, Phys. Rev. A **20**, 1299 (1979).

[9]E. Borie and G. A. Rinker, Phys. Rev. A **18**, 324 (1978); G. Carboni, G. Gorini, G. Torelli, L. Palffy, F. Palmonari, and E. Zavattini, Nucl. Phys. A **278**, 381 (1977). However, recent work has failed to reproduce the μ^--He resonance. See H. P. von Arb, F. Dittus, H. Heeb, H. Hoffer, F. Kottman, S. Niggli, R. Schaeren, D. Taggu, J. Unternahrer, and P. Egelhof, Phys. Lett. B **136**, 232 (1984); M. Eckhause, P. Guss, D. Joyce, J. R. Kane, R. T. Siegel, W. Vulcan, R. E. Welsh, and R. Whyley, Phys. Rev. A **33**, 1743 (1986); J. S. Cohen, *ibid.* **25**, 1791 (1982).

[10]E. Lipworth and R. Novick, Phys. Rev. **108**, 1434 (1957).

[11]M. Narasimham and R. Strombotne, Phys. Rev. A **4**, 14 (1971).

[12]M. Inokuti and Y. Kim, Phys. Rev. **186**, 100 (1969).

[13]F. J. de Heer, in *Advances in Atomic and Molecular Physics,* edited by D. R. Bates and I. Estermann (Academic, New York, 1966), Vol. 2, p. 327.

[14]W. L. Wiess, M. W. Smith, and P. Glennon, *Atomic Transition Probabilities,* Natl. Bur. Stand. Ref. Data Ser. (U.S.) Circ. No. NBS4 (U.S. GPO, Washington, D.C., 1966), Vol. I.

[15]L. B. Lapson and J. G. Timothy, Appl. Opt. **15**, 1218 (1976).

[16]W. R. Ott, W. E. Kaupilla, and W. L. Fite, Phys. Rev. A **1**, 1089 (1970).

[17]F. Nakao, Vacuum **25**, 431 (1975).

[18]P. Pellegrin, Y. El Masri, and L. Palffy, Phys. Rev. A **31**, 5 (1985).

[19]D. R. Wood II, C. K. N. Patel, D. E. Murnick, E. T. Nelson, M. Leventhal, H. W. Kugel, and Y. Niv, Phys. Rev. Lett. **48**, 398 (1982).

[20]H. Gould and R. Marrus, Phys. Rev. A **28**, 2001 (1983).